HHS Public Access

Author manuscript

Hepatology. Author manuscript; available in PMC 2020 December 31.

Published in final edited form as:

Hepatology. 2020 September ; 72(3): 1013–1028. doi:10.1002/hep.31211.

Targeted Apoptosis of Ductular Reactive Cells Reduces Hepatic Fibrosis in a Mouse Model of Cholestasis

Adiba I. Azad[1], **Anuradha Krishnan**[1], **Leia Troop**[1], **Ying Li**[2], **Tomohiro Katsumi**[1], **Kevin Pavelko**[3], **Enis Kostallari**[1], **Maria Eugenia Guicciardi**[1], **Gregory J. Gores**[1]

[1]Division of Gastroenterology and Hepatology, Mayo Clinic, Rochester, MN

[2]Biomedical Statistics and Informatics, Mayo Clinic, Rochester, MN

[3]Department of Immunology, Mayo Clinic, Rochester, MN.

Abstract

BACKGROUND AND AIMS: In cholestatic liver diseases, ductular reactive (DR) cells extend into the hepatic parenchyma and promote inflammation and fibrosis. We have previously observed that multidrug-resistant 2 (*Mdr2*$^{-/-}$) double knockout (DKO) mice lacking tumor necrosis factor–related apoptosis-inducing ligand receptor (*Tr*$^{-/-}$) display a more extensive ductular reaction and hepatic fibrosis compared to *Mdr2*$^{-/-}$ mice. This observation suggests that the magnitude of the DR-cell population may be regulated by apoptosis.

APPROACH AND RESULTS: To examine this concept, we cultured epithelial cell adhesion molecule–positive reactive cholangioids (ERCs) obtained from wild-type (WT), *Tr*$^{-/-}$, *Mdr2*$^{-/-}$ and DKO mice. Single-cell transcriptomics and immunostaining of both WT and DKO ERCs confirmed their DR-cell phenotype. Moreover, DKO ERCs displayed a unique translational cluster with expression of chemokines, indicating a reactive state. Incubation with the myeloid cell leukemia 1 (MCL1) inhibitor S63845, a proapoptotic BH3-mimetic therapy, significantly decreased DKO and *Mdr2*$^{-/-}$ ERC viability compared to WT. Intravenous administration of S63845 significantly reduced the DR-cell population and markers of inflammation and liver fibrosis in *Mdr2*$^{-/-}$ and DKO mice. Furthermore, DKO mice treated with S63845 displayed a significant decrease in hepatic B lymphocytes compared to untreated mice as assessed by high-definition mass cytometry by time-of-flight. Coculture of bone marrow–derived macrophages with ERCs from DKO mouse livers up-regulated expression of the B cell–directed chemokine (C-C motif) ligand 5. Finally, DR cells were noted to be primed for apoptosis with Bcl-2 homologous antagonist/killer activation *in vitro* and *in vivo* in primary sclerosing cholangitis liver specimens.

CONCLUSIONS: DR cells appear to play a key role in recruiting immune cells to the liver to actively create an inflammatory and profibrogenic microenvironment. Pharmacologic targeting of

ADDRESS CORRESPONDENCE AND REPRINT REQUESTS TO: Gregory J. Gores, M.D., Division of Gastroenterology and Hepatology, Mayo Clinic, 200 First Street SW, Rochester, MN 55905, gores.gregory@mayo.edu, Tel.: +1-507-284-0686.

Authors' Contribution: A.I.A., M.E.G. and G.J.G. conceived and designed the study; A.I.A., A.K., L.T., Y.L., T.K., K.P., E.K. and M.E.G. acquired the data; A.I.A., A.K., M.E.G. and G.J.G. analyzed and interpreted the data; A.I.A. drafted the article and A.K., M.E.G. and G.J.G. critically revised it. All authors approved the final version of the article before submission.

Potential conflict of interest: Nothing to report.

Supporting Information

Additional Supporting Information may be found at onlinelibrary.wiley.com/doi/10.1002/hep.31211/suppinfo.

MCL1 in a mouse model of chronic cholestasis reduces DR-cell and B-cell populations and hepatic fibrosis.

The intrahepatic and extrahepatic bile ducts are lined by polarized epithelial cells termed "cholangiocytes." Cholangiocytes modify bile through a transport function, provide a physical barrier between bile duct luminal contents and the adjacent periductal tissue, and engage in crosstalk with other cell types in the periductal space. Unfortunately, bile ducts are affected by inflammation and fibrosis in several human diseases, referred to as the "cholangiopathies."[1,2] These cholangiopathies result in cholestasis (impaired bile formation), which is toxic to the liver, and can result in hepatic fibrosis, cirrhosis, and end-stage liver disease. Collectively, the cholangiopathies are associated with considerable morbidity and mortality. The inflammatory and fibrotic processes mediating the cholangiopathies remain obscure, and accordingly, there is an unmet need for highly effective and mechanism-based therapies.

A histopathologic feature of the cholangiopathies is the emergence of reactive cholangiocytes, which contribute to hepatic inflammation and fibrosis.[3] Reactive cholangiocytes are comprised of two distinct phenotypes, senescent cells and a proliferative ductular reactive (DR)–cell population.[3,4] Although senolytics targeting senescent cells have been explored in cholestasis,[5] therapeutically targeting the proliferative DR-cell population has not been explored. DR cells are epithelial cells characterized by a biliary phenotype, organized into distorted structures, often lacking a lumen, initially localized at the periphery of the portal space, from which they often expand into the hepatic parenchyma.[6] The extension of DR cells from the periportal space to the parenchyma has been termed the "invasive DR-cell phenotype."[7] The origin of DR cells in cholestasis is likely due to expansion of a proliferative cholangiocyte-derived compartment, although other cell types may contribute depending upon the nature of the injury.[8] In human liver diseases, the magnitude of the DR-cell population correlates with the severity of fibrosis in cholestatic liver diseases such as primary sclerosing cholangitis (PSC), strongly suggesting that DR cells promote fibrosis.[6,9-11] However, no studies to date have therapeutically targeted these cells to reduce cholestatic liver injury.

We have explored the apoptotic regulation of the DR-cell population in multidrug resistance 2 (*Mdr2*$^{-/-}$) double knockout (DKO) mice, a murine model of cholestatic liver injury. We crossed *Mdr2*$^{-/-}$ mice with mice genetically lacking the tumor necrosis factor (TNF)–related apoptosis-inducing ligand (TRAIL) receptor (TR), a proapoptotic death receptor, thereby generating *Mdr2*$^{-/-}$*Tr*$^{-/-}$ DKO mice. These mice were characterized by an abundant DR-cell population and correspondingly displayed advanced hepatic injury and fibrosis. Furthermore, we confirmed that the expansion in the DR-cell population in the DKO mice was a result of decreased apoptosis as opposed to an increase in proliferation.[12] These data suggest that TRAIL limits the size of the DR-cell population during cholestasis by inducing apoptosis of this cell phenotype. These DR cells must be primed for apoptosis as healthy epithelial cells (i.e., cholangiocytes) are resistant to TRAIL cytotoxicity. Selected sensitivity to TRAIL generally indicates cells are in a "primed" state, which, in cholangiocytes, is often mediated by the prosurvival BCL2 family protein myeloid cell leukemia 1 (MCL1).[13,14] (Cells primed for apoptosis are uniquely susceptible to proapoptotic stimuli.[15]) Although

exogenous TRAIL administration could represent an approach to reduce the DR-cell population, systemic treatments with exogenous TRAIL agonists are often hepatotoxic,[16] rendering this approach problematic. However, cells primed for cell death are often sensitive to small molecules dubbed “BH3-mimetics,” which bind the BH3 groove of the prosurvival proteins, precluding them from sequestering the proapoptotic BCL2 proteins.[17] In particular, the TRAIL proapoptotic pathway is regulated by MCL1,[13,14] and the BH3-mimetic S63845 has been developed to specifically target MCL1.[18] These observations suggest that S63845 could be used to purposefully induce DR-cell apoptosis to potentially ameliorate cholestatic liver injury.

There are no cell surface markers specific for DR cells; rather, they are characterized phenotypically by morphology and extension into the periportal space of the hepatic lobule *in vivo*, their expression of cholangiocyte differentiation genes (e.g., SRY [sex determining region Y]-box 9 [*Sox9*], keratins 7 and 19 [*Krt7*, *Krt19*], and epithelial cell adhesion molecule [*EpCAM*]), their replicative state, and their reactivity/activation as manifest by expression of cytokines and chemokines.[8,9,19,20] Cholangiocyte-derived organoids (cholangioids) have been developed as a more physiologic three-dimensional (3D) model than traditional two-dimensional cultures.[21] Because DR cells represent a regenerative response to liver injury and organoids are selected for their replicative properties, we reasoned that liver cell–derived organoids could be developed to model several characteristics of DR cells. Toward this goal, we developed cholangioids from an EpCAM-positive liver-cell population as cholangiocytes and DR cells are the predominant EpCAM-positive epithelial cell population in the liver.[22] These cholangioids were obtained from wild-type (WT), $Tr^{-/-}$, $Mdr2^{-/-}$, and DKO mice and displayed characteristics of DR cells with expression of inflammatory chemokines and cytokines. Herein, we characterize these cholangioids in detail and will refer to them as EpCAM-positive reactive cholangioids (ERCs).

Because DR cells exist in a niche with immune cells comprised of macrophages and lymphocytes including B cells, we hypothesized that DR cells must have an immune regulatory role in promoting hepatic inflammation. B lymphocytes have been implicated in promoting hepatic fibrosis in various models of liver injury, including $Mdr2^{-/-}$ mice.[23,24] Distinct subsets of cells with effector and regulatory functions exist within the B-cell population. Effector B cells are considered proinflammatory cells, which secrete cytokines and chemokines, whereas regulatory B cells suppress the inflammatory potential of other immune cells.[25,26] In line with these observations, we aimed to examine whether DR cells directly and/or indirectly affect the immune environment of the liver in mice with chronic cholestasis.

We report that ERCs derived from $Mdr2^{-/-}$ and DKO mice are highly susceptible to S63845-induced apoptosis. More importantly, treatment of $Mdr2^{-/-}$ and DKO mice with S63845 induces apoptosis of the DR cells, thereby diminishing the DR-cell population and reducing hepatic fibrosis.

Methods

ANIMAL STUDIES

All animal procedures were performed in accordance with the Institutional Animal Care and Use Committee of the Mayo Clinic, Rochester, MN. In-house colonies of $Tr^{-/-}$ and $Mdr2^{-/-}$ mice on a C57Bl/6 background were used to generate all genotypes employed for these studies. In brief, $Tr^{-/-}$ mice were crossbred with $Mdr2^{-/-}$ mice to generate heterozygous $Tr^{+/-}Mdr^{+/-}$ animals. Heterozygotes were crossbred to generate the WT, $Tr^{-/-}$, $Mdr2^{-/-}$, and $Tr^{-/-}Mdr2^{-/-}$ (DKO) mice used for multiple experiments, which are described separately. Littermates were used for these studies. All mice were reared on a 12-hour light–dark cycle and had *ad libitum* access to food and water.

GENERATION OF EpCAM-POSITIVE REACTIVE CHOLANGIOIDS

Mouse liver EpCAM (cluster of differentiation 326 [CD326])-positive cells were isolated from WT, $Tr^{-/-}$, $Mdr2^{-/-}$, and DKO mice using a magnetic bead/ affinity antibody approach, as we previously described in detail.[22,27] Organoid growth medium (Supporting Table S1) diluted 1:1 in advanced Dulbecco's modified Eagle's medium containing 1% Glutamax and 10 mM 4-(2-hydroxyethyl)-1-piperazine ethanesulfonic acid was employed to culture the ERCs. ERCs were reseeded in a 1:4 well ratio employing 48-well plates (no. 3548; Corning Costar, Corning, NY).

The remainder of the methods and their corresponding references are included in the Supporting Materials.

Results

CHARACTERIZATION OF ERCs FROM WT, $Tr^{-/-}$, $Mdr2^{-/-}$, AND DKO MICE

Initially, we confirmed that cytokeratin (CK)-19–positive DR cells are increased in the DKO versus $Mdr2^{-/-}$ mouse livers (Fig. 1A,B), consistent with our prior observation.[12] ERCs were obtained and cultured from WT, $Tr^{-/-}$, and $Mdr2^{-/-}$ mice and DKO animals (Fig. 1C). Gene expression profiles associated with cholangiocyte differentiation include *Sox9*, *Krt7*, *Krt19*, and EpCAM.[9] We employed a variety of techniques to ascertain if the ERCs we established and cultured express this genetic profile. First, we performed whole-mount immunofluorescence on ERCs from WT, $Mdr2^{-/-}$, and DKO mice and confirmed expression of CK-7 (Fig. 1D; Supporting Fig. S1A). Representative tile scans used for 3D reconstruction of ERCs are presented (Supporting Fig. S2). Next, we confirmed the absence of senescent cells in the ERCs from the various genotypes by assessing for the marker senescence-associated beta-galactosidase (Fig. 1E). We performed single-cell RNA sequencing on WT and DKO ERCs to characterize the transcriptional heterogeneity within the EpCAM-positive cholangiocyte pool at single-cell resolution. WT and DKO genotypes were chosen to represent the two extremes in DR-cell phenotype as WT animals have virtually no ductular reaction, whereas the DKO mice display a more pronounced DR-cell population (Fig. 1A). We analyzed 2,983 cells from WT and 953 cells from DKO ERCs, which revealed 8 and 6 transcriptionally distinct clusters, respectively (Fig. 1F). The violin plots for cholangiocyte differentiation genes *Krt7*, *Krt19*, and EpCAM exhibit similar

expression levels between the two genotypes (Fig. 1G; Supporting Fig. S1B). Almost all of the clusters in both WT and DKO ERCs displayed expression of genes associated with proliferation as noted by expression of the proliferating cell nuclear antigen gene across clusters (Fig. 1H). Interestingly, DKO ERCs displayed up-regulation in three chemokines, chemokine (C-X-C motif) ligand 1 (*Cxcl1*), *Cxcl2*, and *Cxcl10* in cluster 5 (Fig. 1I). These chemokines were not expressed in WT ERCs. Furthermore, cluster 5 in DKO ERCs displayed a higher expression level of the B cell–recruiting chemokine (C-C motif) ligand 20 (*Ccl20*) than WT ERCs (Fig. 1I). Indeed, CCL20 protein expression analysis by enzyme-linked immunosorbent assay (ELISA) also demonstrated a significantly enhanced expression from DKO ERCs when compared to WT Furthermore, protein expression of cytokines TNFα and interleukin 1 beta (IL-1β), as assessed by ELISA, was also higher in the DKO ERCs (Supporting Fig. S1C,D). Hence, our analysis identifies a transcriptional cell cluster in the DKO ERCs, which demonstrates their ability to generate several chemokines and points to a more highly activated immunoregulatory state than WT ERCs. Therefore, TR signaling may predominantly delete proinflammatory DR cells from the liver.

ERCs FROM *Mdr2*$^{-/-}$ AND DKO MICE ARE ESPECIALLY PRIMED FOR CELL DEATH

TRAIL restrains the DR-cell population in *Mdr2*$^{-/-}$ mice by inducing DR-cell apoptosis as we observed a more pronounced ductular reaction and fibrosis in DKO compared to *Mdr2*$^{-/-}$ mice.[12] Therefore, in the present study we posited that DR cells are primed for cell death given their sensitivity to TRAIL cytotoxicity. To examine this hypothesis, we employed ERCs as models of DR cells. We incubated ERCs from WT, *Tr*$^{-/-}$, *Mdr2*$^{-/-}$, and DKO mice with TRAIL (Fig. 2A). We observed that TRAIL induced cell death in the WT and *Mdr2*$^{-/-}$ ERCs, whereas ERCs from *Tr*$^{-/-}$ and DKO mice were predictably protected from TRAIL. The sensitivity of WT ERCs to TRAIL likely reflects their proliferative phenotype *in vitro.* Next, we employed two specific BH3-mimetics, A1331852, which targets BCLXL, and S63845, which targets MCL1, and examined their effect on ERC viability (Fig. 2B,C) compared to vehicle. WT and *Tr*$^{-/-}$ ERCs displayed a similar response to BCLXL and MCL1 inhibition, with a modest decrease in cell viability (20%-30%) (Fig. 2B,C). However, cell viability in *Mdr2*$^{-/-}$ and DKO ERCs was exquisitely sensitive to MCL1 inhibition (cell viability decrease of 60%-80%) when compared to BCLXL inhibition (cell viability decrease of 0%-20%) (Fig. 2B,C). Consistent with the above findings, WT and *Tr*$^{-/-}$ ERCs displayed no change in caspase 3/7 activity (marker of apoptosis) when exposed to S63845. In contrast, caspase 3/7 activity was markedly increased in *Mdr2*$^{-/-}$ and DKO ERCs treated with S63845 (Fig. 2D,E). Finally, S63845 did not induce cell death in primary hepatocytes and primary hepatic stellate cells (Supporting Fig. S3A,B). Taken together, these studies suggest that ERCs from *Mdr2*$^{-/-}$ and DKO mice are especially primed for apoptosis, which can be induced specifically by pharmacologic inhibition of MCL1.

MECHANISM OF APOPTOSIS PRIMING

The balance between cell survival and cell death is controlled by interactions between the members of the BCL2 family of proteins. In health, prosurvival proteins (e.g., MCL1, BCL2, and BCLXL) bind to and sequester the direct effectors of apoptosis, activated Bcl-2-associated X protein (BAX) and Bcl-2 homologous antagonist/killer (BAK), thereby impairing their ability to oligomerize and form pores that result in mitochondrial outer

membrane permeabilization.[17] To gain a mechanistic insight into the apoptotic predisposition of DR cells, we employed the 603B mouse cholangiocyte cell line. Because the ligand TNF-like weak inducer of apoptosis (TWEAK) is a driver of the ductular reaction in mice,[28] we incubated 603B cells with TWEAK to mimic the ductular reaction phenotype in cell culture. We confirmed by quantitative PCR analysis that TWEAK exposure results in up-regulated expression of genes involved in immunoregulatory and fibrogenesis pathways, *Ccl2*/monocyte chemoattractant protein 1 (*Mcp1*), *Cxcl2*, *Cxcl10*, and transforming growth factor beta (*Tgfβ*), indicating a reactive phenotype (Fig. 3A). This TWEAK-induced reactive phenotype was consistent with the up-regulation of *Cxcl2* and *Cxcl10* gene expression by single-cell RNA-sequencing analysis in cluster 5 of DKO ERCs (Fig. 1H). Next, TWEAK-treated cells were exposed to S63845, and apoptosis was assessed by complementary approaches. Cells exposed to TWEAK displayed a significantly more robust apoptotic response to S63845 than vehicle-treated cells, as demonstrated by caspase 3/7 activity and annexin V positivity analyses (Fig. 3B,C). To identify the molecular mechanism for this apoptotic priming, we investigated whether changes in expression of the BCL2 family of proteins promote apoptosis in TWEAK-treated 603B cells and found no significant difference in the gene or protein expression levels between TWEAK-exposed and unexposed cells (Supporting Fig. S4A,B). Therefore, we performed immunoprecipitation experiments to examine changes in interactions between MCL1 and its proapoptotic binding partners. We observed that TWEAK treatment led to increased binding of BAK to MCL1, indicating BAK activation.[29] This interaction between BAK and MCL1 was disrupted by S63845, consistent with the activity of this BH3-mimetic (Fig. 3D). On the contrary, BAX did not bind MCL1 following incubation with TWEAK (data not shown). These observations highlight the presence of activated BAK following TWEAK stimulation.

To confirm *in vivo* and determine the human relevance for these observations, we employed an antibody specific to the active conformation of BAK[30] to examine the number of $BAK^{+}CK7^{+}$ cells on liver specimens from 3 healthy and 3 PSC patients using immunofluorescence. There were no $BAK^{+}CK7^{+}$ cells identified in healthy livers. On the contrary, liver specimens from patients with PSC displayed presence of $BAK^{+}CK7^{+}$ cells in areas of ductular reaction, as demonstrated in representative immunofluorescent images (Fig. 3E; Supporting Fig. S4C). Based on these results, we infer that DR cells can be primed for apoptosis due to an increased pool of partially activated BAK bound to MCL1, which becomes available to orchestrate apoptosis upon MCL1 inhibition.

THE BH3-MIMETIC S63845 REDUCES THE NUMBER OF DR CELLS AND ATTENUATES HEPATIC FIBROSIS *IN VIVO*

MCL1 inhibition with S63845 has been shown to be specific, potent, safe, and efficacious in preclinical models of hematologic malignancies.[18] To test the effect of MCL1 inhibition on DR cells *in vivo*, we injected $Mdr2^{-/-}$ and DKO mice with 40 mg/kg S63845 or vehicle once daily for 5 consecutive days, a dose previously employed in C57BL/6 mice.[18,31] We observed that treatment with S63845 led to a significant reduction in the DR-cell population in both $Mdr2^{-/-}$ and DKO cohorts (Fig. 4A,B). Accordingly, we observed an increase in terminal deoxynucleotidyl transferase–mediated deoxyuridine triphosphate nick-end labeling (TUNEL)–positive cells in the CK-7 expressing population in the S63845-treated

animals as displayed on representative confocal images (Fig. 4C,D). The mean alanine aminotransferase (ALT) and alkaline phosphatase levels for the untreated and treated mice were not statistically different, indicating that the drug did not induce hepatocellular or biliary tract injury (Supporting Fig. S5A,B). We found that the reduction in the DR-cell population was associated with a robust regression in fibrosis in the *Mdr2*$^{-/-}$ and DKO animals (Fig. 5). Furthermore, expression of alpha smooth muscle actin (αSMA) was significantly reduced in S63845-treated mice (Fig. 5A,C) as demonstrated by immunohistochemistry. Moreover, S63845 treatment significantly decreased levels of profibrogenic and proinflammatory genes in both *Mdr2*$^{-/-}$ and DKO cohorts (Fig. 5B,D). Interestingly, as demonstrated by ELISA analysis, ERCs from *Mdr2*$^{-/-}$ and DKO mouse livers displayed greater levels of TGF-β protein expression compared to WT, suggesting a direct role of DR cells in mediating fibrosis in this model (Fig. 5E). Collectively, these results demonstrate that increased apoptosis of DR cells has a salutary effect on fibrosis in chronic cholestasis. To test the reversibility of MCL1 inhibition, *Mdr2*$^{-/-}$ mice were injected with S63845 for 5 days, euthanized 2 weeks after the last dose, and compared to their untreated littermates. We did not observe any differences in serum ALT (Supporting Fig. S5C) or in the ductular reaction as demonstrated by immunohistochemical analysis of SOX9 and CK-19 (Fig. 6C,D). Notably, S63845-treated mouse livers continued to display a reduction in hepatic fibrosis (Fig. 6A,B). This observation implies that DR-cell apoptosis by S63845 reversibly interrupts an undefined process for regulating the DR-cell population with a lag in fibrogenesis.

REDUCTION IN DR CELLS MODULATES THE LIVER INFLAMMATORY CELL POPULATION

We used high-dimensional mass cytometry by time-of-flight (CyTOF) to profile the intrahepatic leukocyte population which comprises macrophages, B and T lymphocytes, natural killer cells, and neutrophils in DKO mice treated with S63845 or vehicle. Based on the intensities of 24 unique cell surface markers specific for different immune cell type/function (Supporting Fig. S6A,B), 29 clusters were identified (Fig. 7A). These clusters were then used to identify cell types based on marker intensities. We noted a striking difference in the clusters between S63845-treated and untreated samples (Fig. 7B). Most notably, S63845-treated mice displayed a 50% reduction in intrahepatic B lymphocytes (Fig. 7C). There were seven clusters which were specific for B cells (Fig. 7D). The population of B cells had high expression of the B cell–activation marker major histocompatibility complex II (MHCII) (Fig. 7D). Interestingly, a minor subpopulation of B cells (Fig. 7C) was identified by cluster 18 that displayed high levels of T-cell immunoglobulin and mucin domain containing 4 (Tim4), which is associated with a proinflammatory phenotype.[32] A modest increase in the T-cell population was also seen (Supporting Fig. 7A). There were no differences in macrophages, neutrophils, and natural killer cell populations (Supporting Fig. S7A,B). In order to confirm that the B lymphocytes were not systemically depleted by S63845, we performed flow-cytometric analysis on DKO and WT mouse spleens after S63845 treatment and observed no change in the splenic B-lymphocyte population (Fig. 7E; Supporting Fig. S7C,D).

DR CELLS INDUCE MACROPHAGES TO RELEASE PROINFLAMMATORY AND LYMPHOCYTE RECRUITING CHEMOKINES

Initially, we demonstrated by single-cell transcriptomics that DR cells from DKO mouse livers contain a population of cells (cluster 5) that express several immune cell recruiting chemokines including *Ccl20* and increased CCL20 protein expression by ELISA, indicative of an immunoregulatory phenotype (Fig. 1I,J). Our *in vivo* results demonstrate that S63845 results in a reduction in DR cells (Fig. 4) and B-lymphocyte infiltration (Fig. 7). We also confirmed that S63845 does not decrease the pool of B lymphocytes in the spleen (Fig. 7E; Supporting Fig. S7C,D). Moreover, we exposed splenic B cells isolated from DKO mice to conditioned medium derived from WT (control) or DKO ERCs using a two-chamber microfluidic device and quantitatively determined their migration after 18 hours. B cells exposed to conditioned medium from DKO ERCs displayed increased migration relative to control (Supporting Fig. S8). These observations led us to postulate that DR cells likely facilitate B-lymphocyte recruitment directly and indirectly. As macrophages may generate chemokines for B cells, we next cocultured ERCs from WT and DKO mice with bone marrow–derived macrophages (BMDMs) from WT mice. BMDMs cocultured with DKO mice–derived ERCs display an increased expression of several cytokines and chemokines including CCL2, CCL3, CCL4, and CCL5/RANTES (regulated upon activation, normal T cell expressed, and secreted; a B cell–recruiting chemokine[33]) (Fig. 8). These data are consistent with a DR cell–macrophage–B lymphocyte crosstalk mechanism for B lymphocyte recruitment to the liver and suggest a role for DR cells in creating an inflammatory microenvironment in cholestasis. Finally, as B lymphocytes are associated with hepatic fibrogenesis, this may explain why B-lymphocyte depletion reduces hepatic fibrosis in a cholestatic murine model. Thus, reduction in DR cells attenuates an inflammatory, profibrogenic process during cholestasis.

Discussion

The results of this study provide key mechanical insights into the role of DR cells in the pathogenesis of cholestatic liver disease. The principal findings of this study are as follows: (1) ERCs represent a reliable model to study DR cell biology *in vitro*; (2) DR cells are uniquely primed for apoptosis by MCL1 inhibition and, most importantly, (3) MCL1 inhibition *in vivo* significantly reduces the size of the DR-cell population and hepatic fibrosis; and (4) apoptosis of DR cells leads to a reduction of intrahepatic B lymphocytes. These observations are discussed in detail.

ERCs isolated from mouse livers model DR cells *in vivo* due to cell–cell contact and being able to form 3D structures suspended in a scaffold, mimicking in part their hepatic microenvironment. We applied high-resolution tools such as single-cell RNA sequencing of ERCs to characterize these cells in-depth and to shed light on the heterogeneity of their transcriptional states. ERCs, composed of EpCAM-positive cells which almost exclusively display cholangiocyte markers, were taken from the livers of WT and DKO mice, thereby allowing us to evaluate the transcriptomic changes in DR cells in health and pathology (specifically chronic cholestasis). We demonstrate by cluster analysis that both WT and DKO ERCs are composed of several transcriptional states. This observation is in congruence

with previous reports on the heterogeneity of EpCAM-positive primary mouse cholangiocytes.[34] The WT and DKO ERCs shared clusters of cells which have similar transcriptional signatures. However, cluster 5 in DKO was unique in that it expressed a group of transcripts associated with inflammatory signaling, two of which are *Cxcl2* and *Cxcl10,* in agreement with recently published reports[34]; and this cluster was absent in WT, suggesting that a small population of activated cholangiocytes in the DR-cell population may drive pathogenic responses to liver injury. We also note that bile-derived organoids from patients with PSC exhibit an immunomodulatory phenotype.[35]

Apoptosis is tightly regulated by the proapoptotic and prosurvival members of the BCL2 family. The switch from survival to apoptosis is triggered when BH3-only proteins, up-regulated by cellular stress signals, neutralize prosurvival proteins such as MCL1. By removing MCL1's constraint on BAK and BAX, these proapoptotic proteins can oligomerize and execute apoptosis by causing mitochondrial outer membrane permeabilization (MOMP).[17] BH3-mimetics such as S63845 are a class of cancer drugs developed to target apoptosis by tightly binding the surface groove of certain prosurvival members of the BCL2 family, thereby mimicking their natural inhibitors, the BH3-only proteins. Cells which are primed for apoptosis are more sensitive to apoptotic stimuli than others. Priming may be due to increased proportion of prosurvival proteins being loaded with potent activated proapoptotic effectors. This interaction can be disrupted, releasing proapoptotic BAK or BAX. We observed this priming in DR cells by immunoprecipitation experiments on TWEAK-exposed 603B cholangiocytes, where TWEAK leads to increased complexes of MCL1 bound to BAK. Moreover, we confirmed the presence of activated BAK in human PSC liver specimens, confirming the *in vivo* and human relevance of these observations. In the presence of S63845, the unleashing of activated BAK, which is usually sequestered by MCL1,[29] allows BAK to form oligomers leading to MOMP and caspase activation. In this regard, the DR-cell phenotype is primed for apoptosis by the MCL1 targeting BH3-mimetic. We previously showed that senescent cells can be therapeutically targeted by BCLXL inhibition[5]; however, in our studies the ERCs are proliferative and not senescent. Therefore, this DR cell population appears to be sensitized to MCL1 inhibition.

The ductular reaction reflects an aberrant response of cholangiocytes to liver injury.[6] In both experimental and clinical biliary tract injury, DR cells activate hepatic stellate cells and portal fibroblasts directly by secreting TGFβ, platelet-derived growth factor, or vascular endothelial growth factor or can lead to recruitment of neutrophils, macrophages and T cells by producing IL1 beta, IL6, IL8, interferon-gamma, CCL2/MCP-1, and endothelin 1.[8,36] We confirm the activated state of TWEAK-exposed 603B cholangiocytes and DKO ERCs when compared to untreated cells and WT ERCs, respectively. The profibrogenic characteristics of DR cells are further suggested by studies which show a strong association between ductular reaction and portal fibrosis in various models of liver disease.[9,37-39] We report that specifically targeting DR cells by the MCL1 inhibitor S63845 results in a robust reduction in DR cells and fibrosis in *Mdr2*$^{-/-}$ and DKO mice. We performed an in-depth profiling of the hepatic immune cell population in DKO mice and demonstrate that DKO mouse livers contain B lymphocytes which are enriched in MHCII, a marker of B-cell activation.[40] Furthermore, a small subset of B cells enriched in Tim4 was identified. This phenotype has been identified as proinflammatory B cells.[32] These B lymphocytes are

dramatically reduced when the DKO mice are treated with S63845. B lymphocytes have been shown to promote fibrosis in various models.[23,24] We show by single-cell transcriptomics and ELISA analysis for protein that the DR-cell population consists of a subset of cells which express several chemokines including the B-cell chemoattractant *Ccl20*.[41,42] Furthermore, we demonstrate by coculture experiments that DR cells can induce macrophages to generate cytokines and chemokines involved in B-cell activation and recruitment.[33,43] The results of these complementary experiments suggest a role of DR cells in orchestrating an immunomodulatory microenvironment.

In conclusion, our findings indicate that targeted apoptosis of DR cells is salutary in mouse models of chronic cholestasis. Despite the importance of MCL1 in different tissues as noted by the results of genetic knockout of MCL1,[44-46] S63845 surprisingly is not associated with significant lasting toxicity in mice.[18] MCL1 is a promising target in cancer therapy, and S63845 has been developed as an anticancer agent. We speculate that MCL1 inhibition may be beneficial in human cholestatic liver diseases.

Supplementary Material

Refer to Web version on PubMed Central for supplementary material.

Acknowledgment:

The administrative assistance of Ms. Courtney Hoover is much appreciated. We appreciate the technical assistance of Dr. A. Revzin and Dr. Y. Gao, Department of Physiology and Biomedical Engineering, Mayo Clinic, Rochester, MN, for the microfluidic chamber studies.

Grant Support: This work was supported by the National Institutes of Health (DK124182, to G.J.G.); P30DK084567, to the optical microscopy core of the Mayo Clinic Center for Cell Signaling in Gastroenterology), National Cancer Institute's Cancer Center (5P30 CA15083-43C1, to the Mayo Clinic Medical Genome Facility–Proteomics Core); T32 DK07198, the Chris M. Carlos and Catharine Nicole Jockisch Carlos Endowment Fund in PSC.

Abbreviations:

BAK	Bcl-2 homologous antagonist/killer
BAX	Bcl-2-associated X protein
BMDM	bone marrow–derived macrophages
CCL	chemokine (C-C motif) ligand
CD	cluster of differentiation
CK	cytokeratin
Cxcl	chemokine (C-X-C motif) ligand
CyTOF	mass cytometry by time-of-flight
3D	three-dimensional
DKO	double knockout

DR	ductular reactive
ELISA	enzyme-linked immunosorbent assay
EpCAM	epithelial cell adhesion molecule
ERC	EpCAM positive reactive cholangioids
IL	interleukin
Krt7/Krt19	keratins 7 and 19
MCL1	myeloid cell leukemia 1
MCP1	monocyte chemoattractant protein 1
Mdr2	multidrug resistant 2
MHCII	major histocompatibility complex
PSC	primary sclerosing cholangitis
SMA	alpha–smooth muscle actin
SOX9	SRY (sex determining region Y)-box 2
***TGF*β**	transforming growth factor beta
Tim4	T-cell immunoglobulin and mucin domain containing 4
TNF	tumor necrosis factor
TR	TRAIL receptor
TRAIL	tumor necrosis factor–related apoptosis-inducing ligand
TUNEL	terminal deoxynucleotidyl transferase–mediated deoxyuridine triphosphate nick-end labeling
TWEAK	TNF-like weak inducer of apoptosis
WT	wild type

REFERENCES

1). Lazaridis KN, LaRusso NF. The cholangiopathies. Mayo Clin Proc 2015;90:791–800. [PubMed: 25957621]
2). Lazaridis KN, LaRusso NF. Primary sclerosing cholangitis. N Engl J Med 2016;375:1161–1170. [PubMed: 27653566]
3). Guicciardi ME, Trussoni CE, LaRusso NF, Gores GJ. The spectrum of reactive cholangiocytes in primary sclerosing cholangitis. HEPATOLOGY 2020;71:741–748. [PubMed: 31833071]
4). Popper H, Kent G, Stein R. Ductular cell reaction in the liver in hepatic injury. J Mt Sinai Hosp N Y 1957;24:551–556. [PubMed: 13476145]
5). Moncsek A, Al-Suraih MS, Trussoni CE, O'Hara SP, Splinter PL, Zuber C, et al. Targeting senescent cholangiocytes and activated fibroblasts with B-cell lymphoma-extra large inhibitors

ameliorates fibrosis in multidrug resistance 2 gene knockout (Mdr2$^{-/-}$) mice. HEPATOLOGY 2018;67:247–259. [PubMed: 28802066]

6). Fabris L, Spirli C, Cadamuro M, Fiorotto R, Strazzabosco M. Emerging concepts in biliary repair and fibrosis. Am J Physiol Gastrointest Liver Physiol 2017;313:G102–G116. [PubMed: 28526690]

7). Clerbaux LA, Manco R, Van Hul N, Bouzin C, Sciarra A, Sempoux C, et al. Invasive ductular reaction operates hepatobiliary junctions upon hepatocellular injury in rodents and humans. Am J Pathol 2019;189:1569–1581. [PubMed: 31108103]

8). Alvaro D, Mancino MG, Glaser S, Gaudio E, Marzioni M, Francis H, et al. Proliferating cholangiocytes: a neuroendocrine compartment in the diseased liver. Gastroenterology 2007;132:415–431. [PubMed: 17241889]

9). Sato K, Marzioni M, Meng F, Francis H, Glaser S, Alpini G. Ductular reaction in liver diseases: pathological mechanisms and translational significances. HEPATOLOGY 2019;69:420–430. [PubMed: 30070383]

10). Williams MJ, Clouston AD, Forbes SJ. Links between hepatic fibrosis, ductular reaction, and progenitor cell expansion. Gastroenterology 2014;146:349–356. [PubMed: 24315991]

11). Crosby HA, Hubscher S, Fabris L, Joplin R, Sell S, Kelly D, et al. Immunolocalization of putative human liver progenitor cells in livers from patients with end-stage primary biliary cirrhosis and sclerosing cholangitis using the monoclonal antibody OV-6. Am J Pathol 1998;152:771–779. [PubMed: 9502419]

12). Krishnan A, Katsumi T, Guicciardi ME, Azad AI, Ozturk NB, Trussoni CE, Gores GJ. TRAIL receptor deficiency promotes the ductular reaction, macrophage accumulation and hepatic fibrosis in the Mdr2$^{-/-}$ mouse. J Pathol 2020.

13). Woo SM, Min KJ, Seo BR, Kwon TK. YM155 sensitizes TRAIL-induced apoptosis through cathepsin S-dependent down-regulation of Mcl-1 and NF-kappaB-mediated down-regulation of c-FLIP expression in human renal carcinoma Caki cells. Oncotarget 2016;7:61520–61532. [PubMed: 27528031]

14). Han MA, Min KJ, Woo SM, Seo BR, Kwon TK. Eupafolin enhances TRAIL-mediated apoptosis through cathepsin S-induced down-regulation of Mcl-1 expression and AMPK-mediated Bim up-regulation in renal carcinoma Caki cells. Oncotarget 2016;7:65707–65720. [PubMed: 27582546]

15). Singh R, Letai A, Sarosiek K. Regulation of apoptosis in health and disease: the balancing act of BCL-2 family proteins. Nat Rev Mol Cell Biol 2019;20:175–193. [PubMed: 30655609]

16). Takeda K, Kojima Y, Ikejima K, Harada K, Yamashina S, Okumura K, et al. Death receptor 5 mediated-apoptosis contributes to cholestatic liver disease. Proc Natl Acad Sci U S A 2008;105:10895–10900. [PubMed: 18667695]

17). Adams JM, Cory S. The BCL-2 arbiters of apoptosis and their growing role as cancer targets. Cell Death Differ 2018;25:27–36. [PubMed: 29099483]

18). Kotschy A, Szlavik Z, Murray J, Davidson J, Maragno AL, Le Toumelin-Braizat G, et al. The MCL1 inhibitor S63845 is tolerable and effective in diverse cancer models. Nature 2016;538:477–482. [PubMed: 27760111]

19). Carpino G, Cardinale V, Folseraas T, Overi D, Floreani A, Franchitto A, et al. Hepatic stem/progenitor cell activation differs between primary sclerosing and primary biliary cholangitis. Am J Pathol 2018;188:627–639. [PubMed: 29248458]

20). Zhou T, Kyritsi K, Wu N, Francis H, Yang Z, Chen L, et al. Knockdown of vimentin reduces mesenchymal phenotype of cholangiocytes in the Mdr2$^{-/-}$ mouse model of primary sclerosing cholangitis (PSC). EBioMedicine 2019;48:130–142. [PubMed: 31522982]

21). Loarca L, De Assuncao TM, Jalan-Sakrikar N, Bronk S, Krishnan A, Huang B, et al. Development and characterization of cholangioids from normal and diseased human cholangiocytes as an in vitro model to study primary sclerosing cholangitis. Lab Invest 2017;97:1385–1396. [PubMed: 28892096]

22). Katsumi T, Guicciardi ME, Azad A, Bronk SF, Krishnan A, Gores GJ. Activated cholangiocytes release macrophage-polarizing extracellular vesicles bearing the DAMP S100A11. Am J Physiol Cell Physiol 2019;317:C788–C799. [PubMed: 31365294]

23). Novobrantseva TI, Majeau GR, Amatucci A, Kogan S, Brenner I, Casola S, et al. Attenuated liver fibrosis in the absence of B cells. J Clin Invest 2005;115:3072–3082. [PubMed: 16276416]

24). Faggioli F, Palagano E, Di Tommaso L, Donadon M, Marrella V, Recordati C, et al. B lymphocytes limit senescence-driven fibrosis resolution and favor hepatocarcinogenesis in mouse liver injury. HEPATOLOGY 2018;67:1970–1985. [PubMed: 29105104]

25). Lund FE, Randall TD. Effector and regulatory B cells: modulators of $CD4^+$ T cell immunity. Nat Rev Immunol 2010;10:236–247. [PubMed: 20224569]

26). Shen P, Fillatreau S. Antibody-independent functions of B cells: a focus on cytokines. Nat Rev Immunol 2015;15:441–451. [PubMed: 26065586]

27). Lu WY, Bird TG, Boulter L, Tsuchiya A, Cole AM, Hay T, et al. Hepatic progenitor cells of biliary origin with liver repopulation capacity. Nat Cell Biol 2015;17:971–983. [PubMed: 26192438]

28). Bird TG, Lu WY, Boulter L, Gordon-Keylock S, Ridgway RA, Williams MJ, et al. Bone marrow injection stimulates hepatic ductular reactions in the absence of injury via macrophage-mediated TWEAK signaling. Proc Natl Acad Sci U S A 2013;110:6542–6547. [PubMed: 23576749]

29). Dai H, Ding H, Meng XW, Peterson KL, Schneider PA, Karp JE, "et al. Constitutive BAK activation as a determinant of drug sensitivity in malignant lymphohematopoietic cells. Genes Dev 2015;29:2140–2152. [PubMed: 26494789]

30). Alsop AE, Fennell SC, Bartolo RC, Tan IK, Dewson G, Kluck RM. Dissociation of Bak alpha1 helix from the core and latch domains is required for apoptosis. Nat Commun 2015;6:6841. [PubMed: 25880232]

31). Brennan MS, Chang C, Tai L, Lessene G, Strasser A, Dewson G, et al. Humanized Mcl-1 mice enable accurate preclinical evaluation of MCL-1 inhibitors destined for clinical use. Blood 2018;132:1573–1583. [PubMed: 30139826]

32). Ding Q Mohib K, Kuchroo VK, Rothstein DM. TIM-4 identifies IFN-gamma-expressing proinflammatory B effector 1 cells that promote tumor and allograft rejection. J Immunol 2017;199:2585–2595. [PubMed: 28848066]

33). Hu Y, Zhang H, Li J, Cong X, Chen Y, He G, et al. Gut-derived lymphocyte recruitment to liver and induce liver injury in non-alcoholic fatty liver disease mouse model. J Gastroenterol Hepatol 2016;31:676–684. [PubMed: 26430807]

34). Planas-Paz L, Sun T, Pikiolek M, Cochran NR, Bergling S, Orsini V, et al. YAP, but Not RSPO-LGR4/5, signaling in biliary epithelial cells promotes a ductular reaction in response to liver injury. Cell Stem Cell 2019;25:39–53.e10. [PubMed: 31080135]

35). Soroka CJ, Assis DN, Alrabadi LS, Roberts S, Cusack L, Jaffe AB, et al. Bile-derived organoids from patients with primary sclerosing cholangitis recapitulate their inflammatory immune profile. HEPATOLOGY 2019;70:871–882. [PubMed: 30561836]

36). Isse K, Harada K, Nakanuma Y. IL-8 expression by biliary epithelial cells is associated with neutrophilic infiltration and reactive bile ductules. Liver Int 2007;27:672–680. [PubMed: 17498253]

37). Clouston AD, Powell EE, Walsh MJ, Richardson MM, Demetris AJ, Jonsson JR. Fibrosis correlates with a ductular reaction in hepatitis C: roles of impaired replication, progenitor cells and steatosis. HEPATOLOGY 2005;41:809–818. [PubMed: 15793848]

38). Fickert P, Stoger U, Fuchsbichler A, Moustafa T, Marschall HU, Weiglein AH, et al. A new xenobiotic-induced mouse model of sclerosing cholangitis and biliary fibrosis. Am J Pathol 2007;171:525–536. [PubMed: 17600122]

39). Richardson MM, Jonsson JR, Powell EE, Brunt EM, Neuschwander-Tetri BA, Bhathal PS, et al. Progressive fibrosis in nonalcoholic steatohepatitis: association with altered regeneration and a ductular reaction. Gastroenterology 2007;133:80–90. [PubMed: 17631134]

40). Yuseff MI, Pierobon P, Reversat A, Lennon-Dumenil AM. How B cells capture, process and present antigens: a crucial role for cell polarity. Nat Rev Immunol 2013;13:475–486. [PubMed: 23797063]

41). Armas-Gonzalez E, Dominguez-Luis MJ, Diaz-Martin A, Arce-Franco M, Castro-Hernandez J, Danelon G, et al. Role of CXCL13 and CCL20 in the recruitment of B cells to inflammatory foci in chronic arthritis. Arthritis Res Ther 2018;20:114. [PubMed: 29880013]

42). Paradis M, Mindt BC, Duerr CU, Rojas OL, Ng D, Boulianne B, et al. A TNF-alpha-CCL20-CCR6 axis regulates Nod1-induced B cell responses. J Immunol 2014;192:2787–2799. [PubMed: 24534531]

43). Burger JA, Quiroga MP, Hartmann E, Burkle A, Wierda WG, Keating MJ, et al. High-level expression of the T-cell chemokines CCL3 and CCL4 by chronic lymphocytic leukemia B cells in nurselike cell cocultures and after BCR stimulation. Blood 2009;113:3050–3058. [PubMed: 19074730]

44). Opferman JT, Iwasaki H, Ong CC, Suh H, Mizuno S, Akashi K, et al. Obligate role of anti-apoptotic MCL-1 in the survival of hematopoietic stem cells. Science 2005;307:1101–1104. [PubMed: 15718471]

45). Thomas RL, Roberts DJ, Kubli DA, Lee Y, Quinsay MN, Owens JB, et al. Loss of MCL-1 leads to impaired autophagy and rapid development of heart failure. Genes Dev 2013;27:1365–1377. [PubMed: 23788623]

46). Wang X, Bathina M, Lynch J, Koss B, Calabrese C, Frase S, et al. Deletion of MCL-1 causes lethal cardiac failure and mitochondrial dysfunction. Genes Dev 2013;27:1351–1364. [PubMed: 23788622]

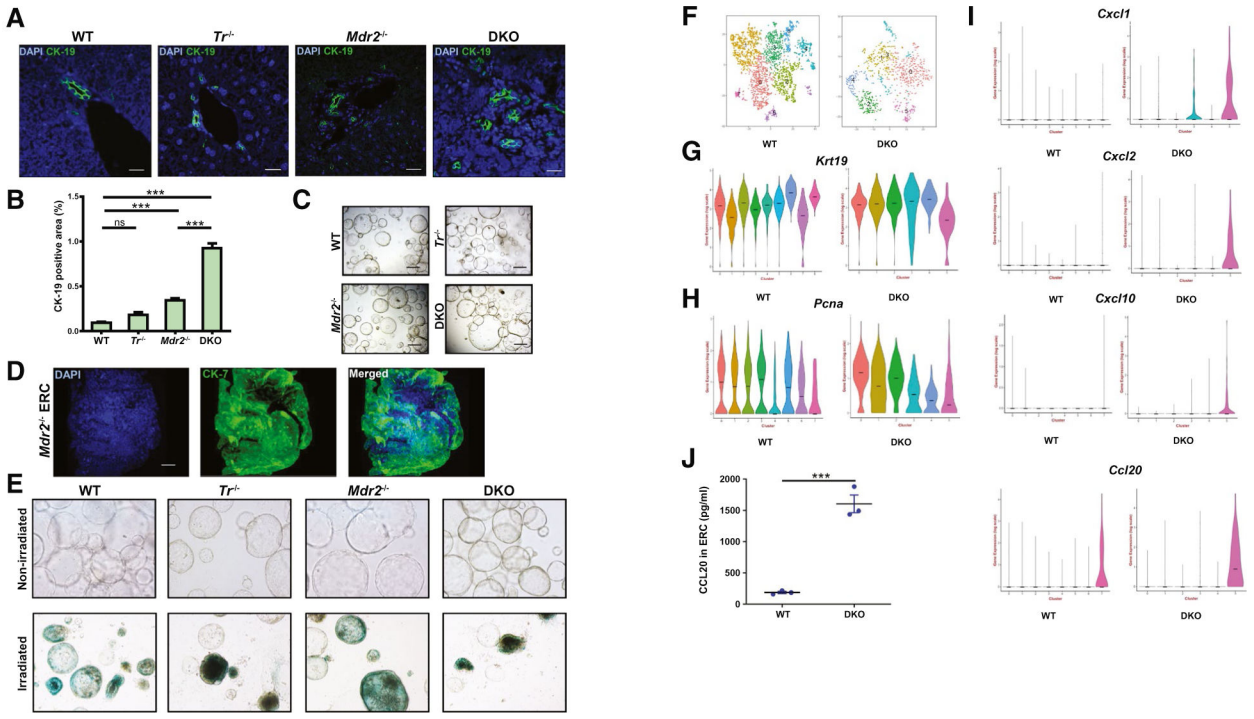

FIG. 1.

Characterization and identification of subpopulations of cholangiocytes in ERCs. (A) Representative immunofluorescent images (40x) of mouse liver tissue stained for CK-19 (green) and DAPI (blue). Scale bar, 20 μm. (B) Quantitative morphometry for CK-19-positive area (n = 3-8). (C) Representative bright field images (10) of cultured ERCs from WT, *Tr*$^{-/-}$, *Mdr2*$^{-/-}$, and DKO mice. Scale bar, 500 μm. (D) Whole mount immunofluorescence (40x) of *Mdr2*$^{-/-}$ ERCs stained with CK-7 (green) and DAPI (blue) represented as 3D image reconstruction from Z stacks 50 μm in thickness. Scale bar, 50 μm (E) Representative bright field images (20x) of senescence associated-β-galactosidase staining (blue) on cultured WT, *Tr*$^{-/-}$, *Mdr2*$^{-/-}$, and DKO ERCs (upper panel) using irradiated ERCs as control (lower panel). (F-I) Single-cell transcriptomic analyses. (F) T-distributed stochastic neighbor embedding maps of the clusters in WT (2,983 cells) and DKO (953 cells) ERCs as analyzed by Seurat. Colors represent unique cell population clusters as identified by gene transcript signature. (G-H) Violin plots comparing transcript levels of (G) *Krt19*, (H) proliferating cell nuclear antigen, and (I) chemokines detected in WT and DKO ERCs. Transcript counts are expressed in logarithmic scale. (J) ELISA analysis of CCL20 from medium collected from WT and DKO ERCs (n = 3 in duplicate). Data are expressed as mean ± SEM. ***$P < 0.005$. Abbreviations: DAPI, 4′,6-diamidino-2-phenylindole; ns, not significant; Pcna, proliferating cell nuclear antigen.

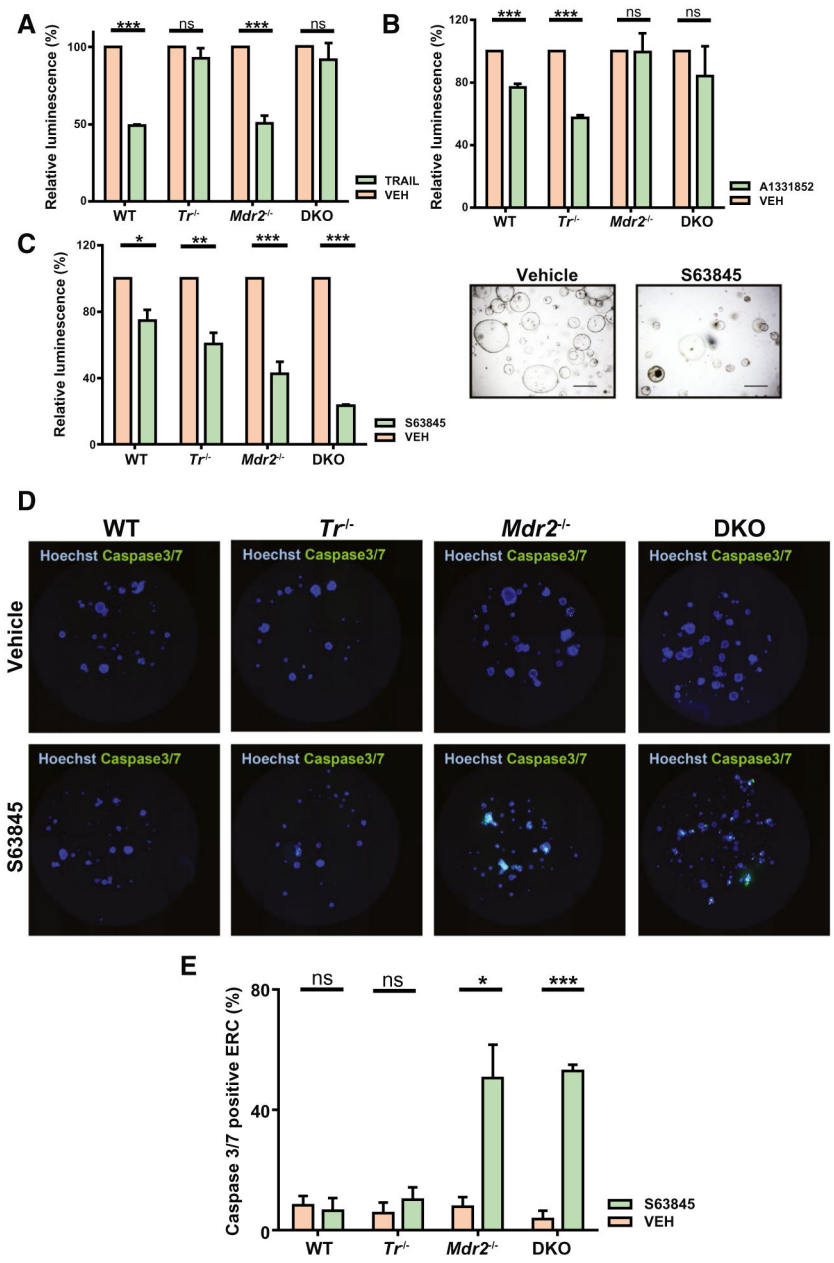

FIG. 2.

Ductular reactive cells are primed for cell death. Cell viability was analyzed by CellTiter Glo 3D luminescent assay in the following experiments. (A) ERCs were exposed to vehicle or TRAIL (10 ng/mL) for 24 hours, and cell viability was assessed (n = 3). (B) ERCs were exposed to vehicle or A1331852 (10 μM) for 48 hours, and cell viability was assessed (n ≥ 3). (C) ERCs were exposed to vehicle or S63845 (10 μM) for 48 hours, and cell viability was assessed (n ≥ 3). Images on the right represent bright field views (10x) of DKO ERCs untreated (left) and treated (right) with S63845 (10 μM) for 48 hours. (D,E) ERCs were incubated with vehicle (upper panel) or S63845 (10 μM) for 48 hours, stained for caspase3/7 (green) and Hoechst (blue), and analyzed on a Celigo Image Cytometer. Representative 96 whole-well fluorescent overlay images of caspase3/7 and Hoechst are

shown with (E) quantitative analysis of percentage of caspase 3/7-positive ERCs (n ≥ 3). Data are expressed as mean ± SEM. *$P < 0.05$, ***$P < 0.005$. Abbreviations: ns, not significant; VEH, vehicle.

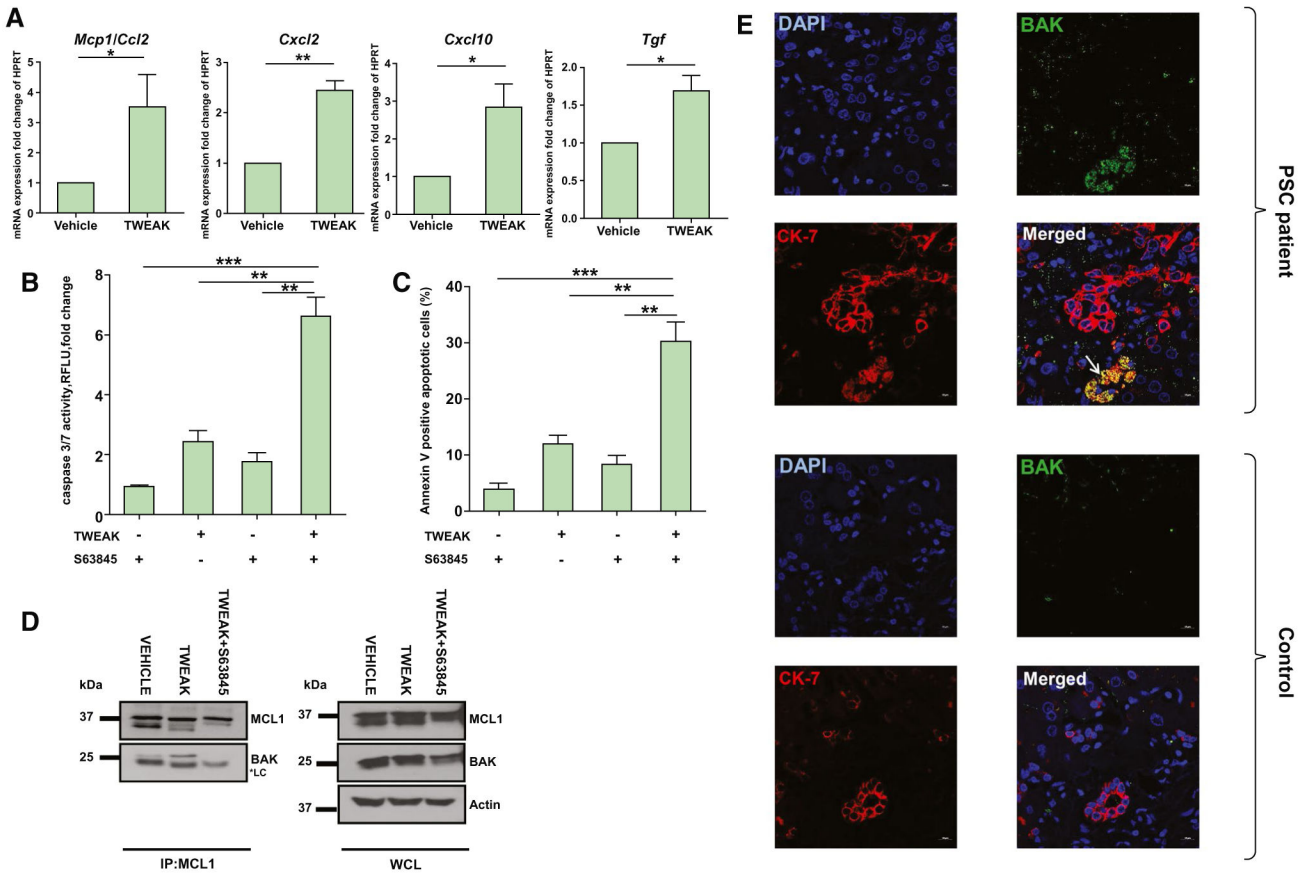

FIG. 3.

DR cells are primed for cell death by increased binding of BAK to MCL1. (A) 603B cholangiocytes were incubated with TWEAK (200 ng/mL) for 48 hours, and expression of proinflammatory genes was analyzed by quantitative real-time PCR (n = 3). (B,C) 603B cholangiocytes were incubated with TWEAK (200 ng/mL) for 48 hours, then S63845 (10 μM) for an additional 24 hours; and apoptosis was assessed by (B) caspase 3/7 activity and (C) annexin V positivity (n = 3). (D) 603B cholangiocytes were incubated with TWEAK (200 ng/mL) for 48 hours or TWEAK (200 ng/mL) for 48 hours followed by S63845 (10 μM) for an additional 24 hours. MCL1 was immunoprecipitated, and association with BAK was assessed by immunoblot. Actin was used as loading control. (E) Representative images of CK-7 (red) and activated BAK (green) coimmunofluorescence (yellow) on stage 3 PSC (upper panel) and healthy (control) human liver specimens (lower panel). White arrow points to location of $BAK^{+}CK7^{+}$ cells. 40x lens, 1.5 magnification. Scale bars, 10 μm. Data are expressed as mean ± SEM. $*P < 0.05$, $**P < 0.01$, $***P < 0.005$. Abbreviations: DAPI, 4′,6-diamidino-2-phenylindole; HPRT, hypoxanthine-guanine phosphoribosyltransferase; IP, immunoprecipitation; Mcp1, monocyte chemoattractant protein 1; RFLU, relative fluorescence units; WCL, whole-cell lysate.

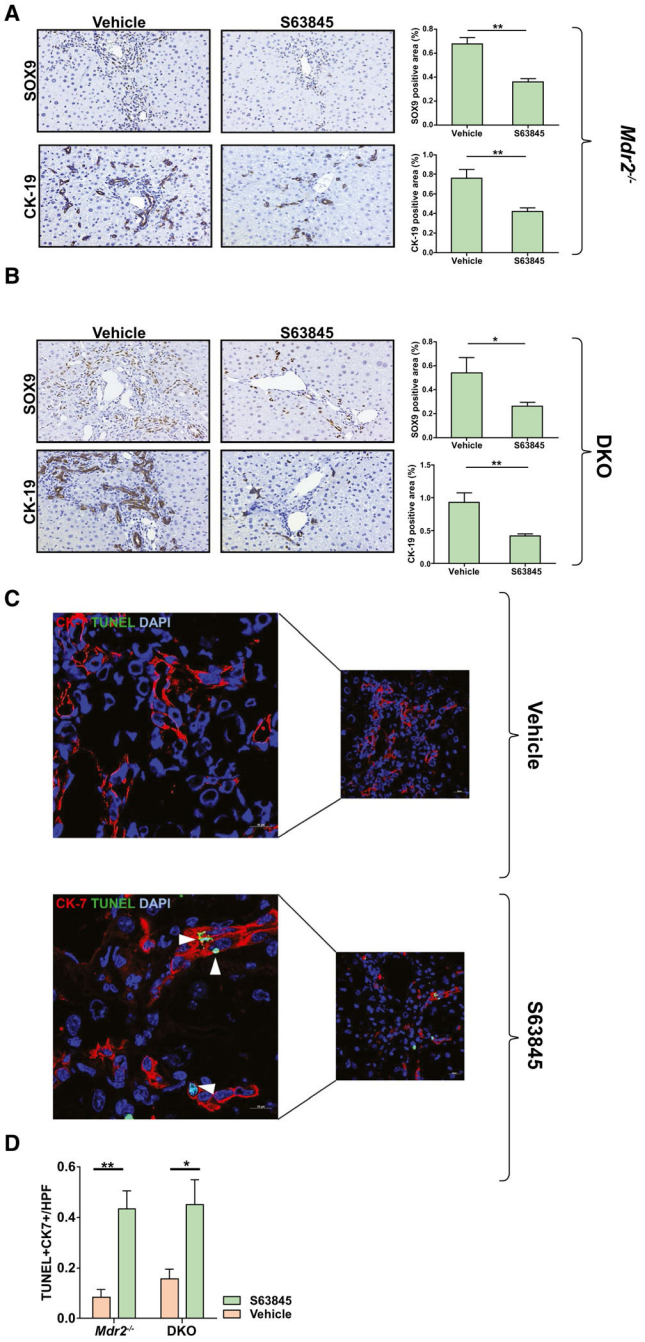

FIG. 4.

MCL1 inhibition by S63845 reduces the DR cell population in *Mdr2*$^{-/-}$ and DKO mice. Mice were treated with vehicle or S63845 (40 mg/kg) daily for 5 days by tail vein injection and euthanized within 24 hours from the last dose. (A) Immunoreactivity for markers of ductular reaction, SOX9 and CK-19, was assessed by immunohistochemistry in *Mdr2*$^{-/-}$ mouse livers (n = 6). (B) Immunoreactivity for SOX9 and CK-19 was assessed in DKO mouse livers (n = 6-8). Graphs represent the respective SOX9 and CK-19 quantifications. (C) DR cell apoptosis in vehicle and S63845-treated *Mdr2*$^{-/-}$ and DKO mice was assessed

by CK-7^{+}TUNEL^{+} cells. Representative images (40x) of liver sections stained with CK-7 (red) and TUNEL (green). Higher magnifications of the images are presented on the left. White arrowheads point to TUNEL-positive cholangiocytes. (D) Graph represents the number of TUNEL^{+}CK7^{+} cells per high-power field averaged from 10 fields per mouse tissue (n = 6). Data are expressed as mean ± SEM. *$P < 0.05$, **$P < 0.01$. Abbreviations: DAPI, 4′,6-diamidino-2-phenylindole; HPF, high-power field.

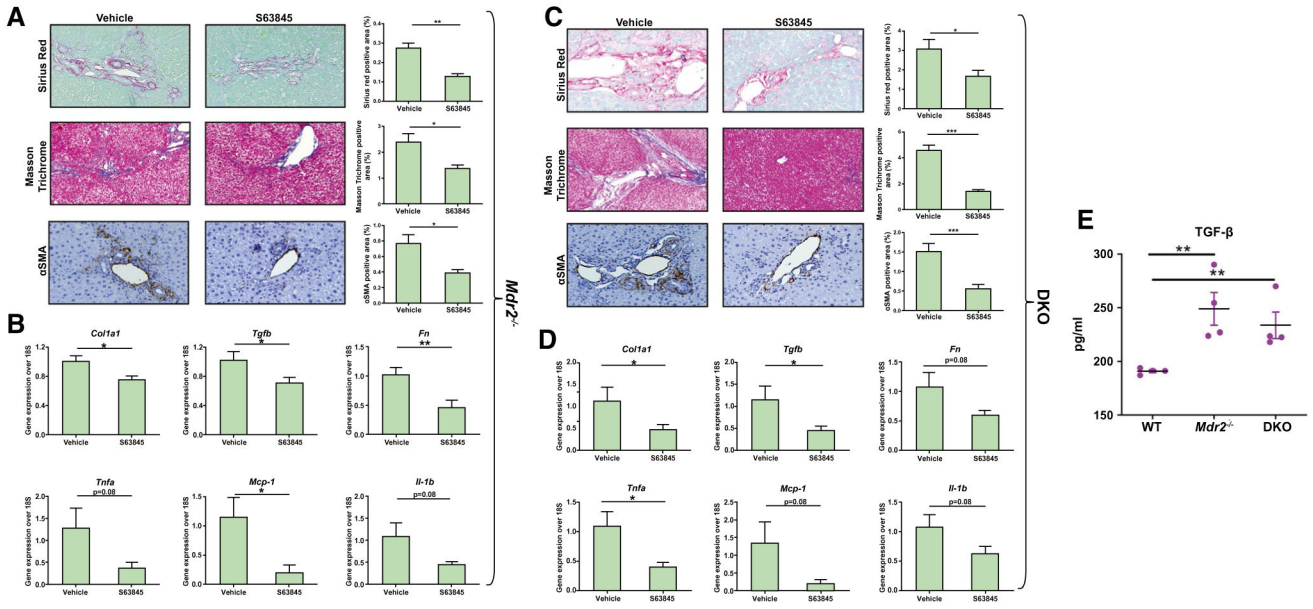

FIG. 5.

MCL1 inhibition by S63845 decreases hepatic fibrosis in *Mdr2*$^{-/-}$ and DKO mice. Mice were treated with vehicle or S63845 (40 mg/kg) daily for 5 days by tail vein injection and euthanized within 24 hours from the last dose. Liver sections and whole liver RNA of (A,B) *Mdr2*$^{-/-}$ and (C,D) DKO mice were examined for markers of fibrosis and inflammation. (A,C) Collagen deposition with sirius red (20x), Masson-trichrome staining (20x), and immunoreactivity for marker of activated fibroblasts αSMA (20x) where indicated. Graphs on the right of the histological images show their respective quantitative morphometry (n = 6-8). (B,D). Gene expression analysis of hepatic fibrosis and inflammation markers (n = 4-7). (E) ELISA analysis of TGFβ from medium from WT, *Mdr2*$^{-/-}$, and DKO ERCs (n = 4 in duplicate). Data are expressed as mean ± SEM. **P* < 0.05, ***P* < 0.01, ****P* < 0.005. Abbreviations: Col1a1, collagen type I alpha 1 chain; Fn, fibronectin.

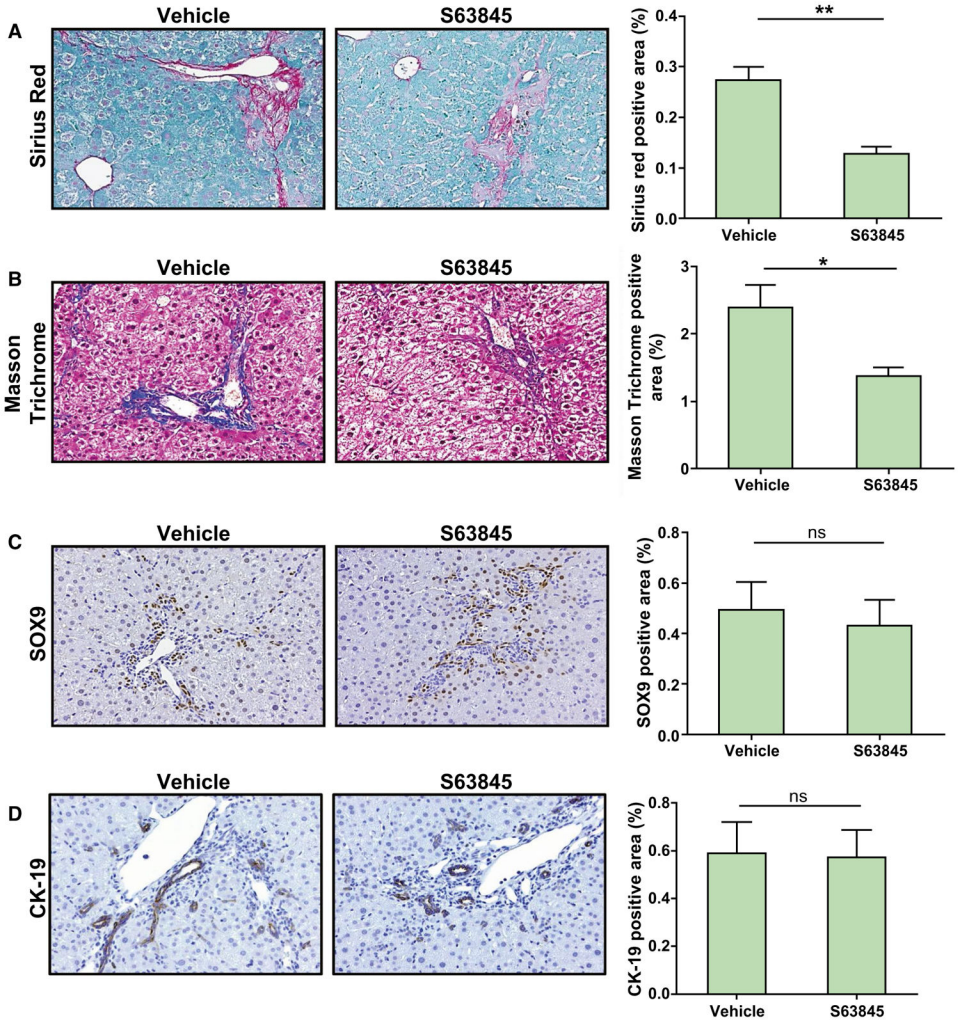

FIG. 6.

Reduction in hepatic fibrosis is sustained after treatment with S63845. *Mdr2*$^{-/-}$ mice were treated with vehicle or S63845 (40 mg/kg) daily for 5 days by tail vein injection and euthanized 2 weeks after the last dose. Liver sections were examined for collagen deposition with (A) sirius red (20x) and (B) Masson-trichrome staining (20x). (C,D) Ductular reaction was examined by immunoreactivity for (C) SOX9 (20x) and (D) CK-19 (20x). Graphs on the right of the histological images show their respective quantitative morphometry (n = 3). Data are expressed as mean ± SEM. *$P < 0.05$, **$P < 0.01$. Abbreviation: ns, not significant.

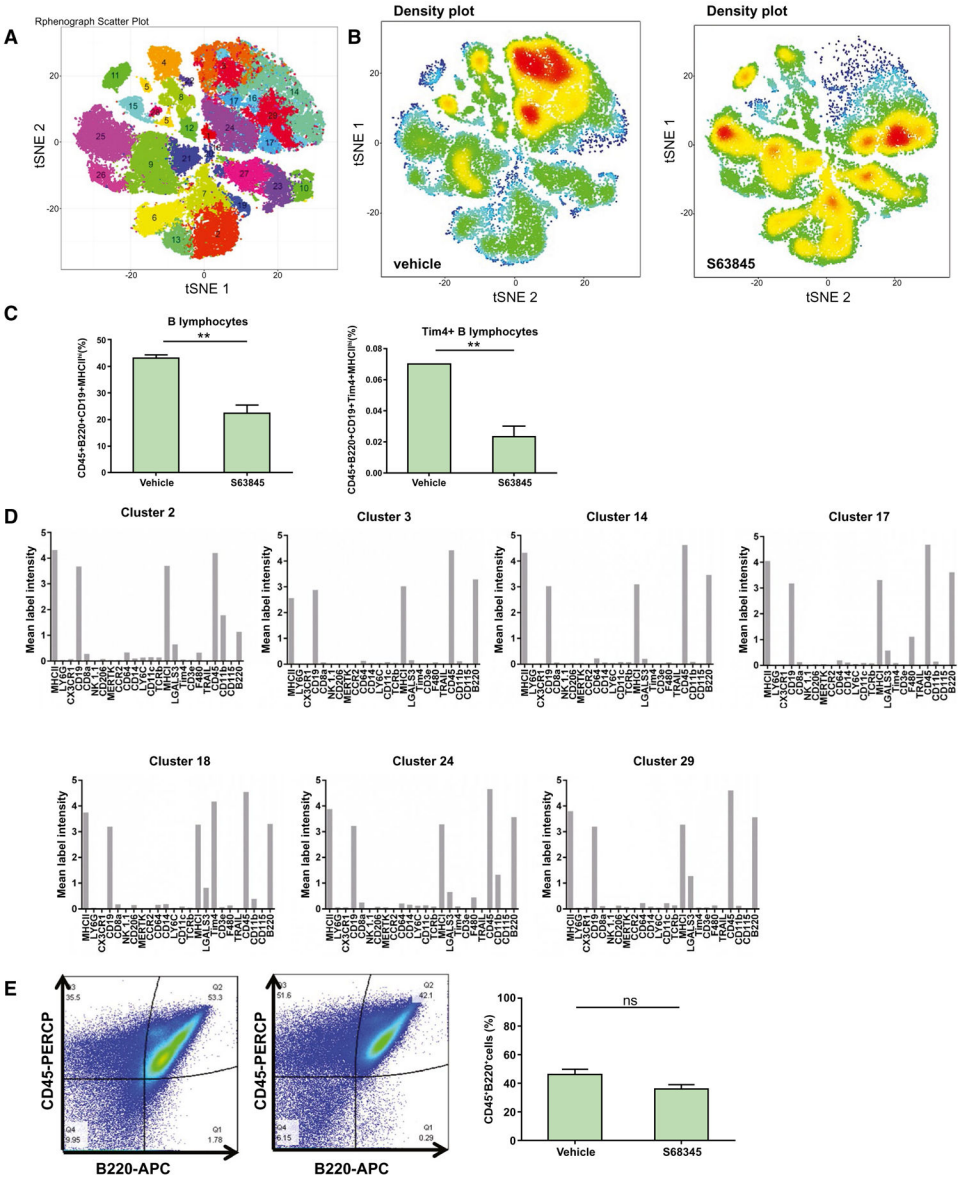

FIG. 7.

S63845 treatment reduces the intrahepatic B lymphocyte population and does not deplete the systemic pool of B lymphocytes. Intrahepatic leukocytes from DKO mice treated with vehicle or S63845 (40 mg/kg) daily for 5 days were stained with a panel of 24 cell surface markers and analyzed by CyTOF (n = 3). (A) Twenty-nine distinct clusters of intrahepatic leukocytes are visualized on a t-distributed stochastic neighbor embedding plot. (B) Representative density plots of vehicle and S63845-treated groups displaying the change in clusters. Red indicates high frequency categorization of cells to a cluster; blue indicates low frequency. (C) Distribution of B cells across clusters which were identified by $CD45^{+}B220^{+}CD19^{+}MHCIIhi$ (B lymphocytes) and $CD45^{+}B220+CD19^{+}Tim4^{+}MHCIIhi$ (a proinflammatory B-cell cluster). (D) Seven clusters that identified B cells, including cluster 18, which was specific for the proinflammatory phenotype. (E) DKO mice were treated with vehicle or S63845 (40 mg/kg) daily for 5 days, and spleens were harvested. Representative

fluorescence-activated cell sorting analysis of primary splenic cells showing single $CD45^{+}B220^{+}$ cells (B lymphocytes). Graph represents the percentage of B lymphocytes (n = 3). Data are expressed as mean ± SEM. $*P < 0.05$, $**P < 0.01$. Abbreviations: APC, allophycocyanin; ns, not significant; PERCP, peridinin chlorophyll protein; tSNE, t-distributed stochastic neighbor embedding.

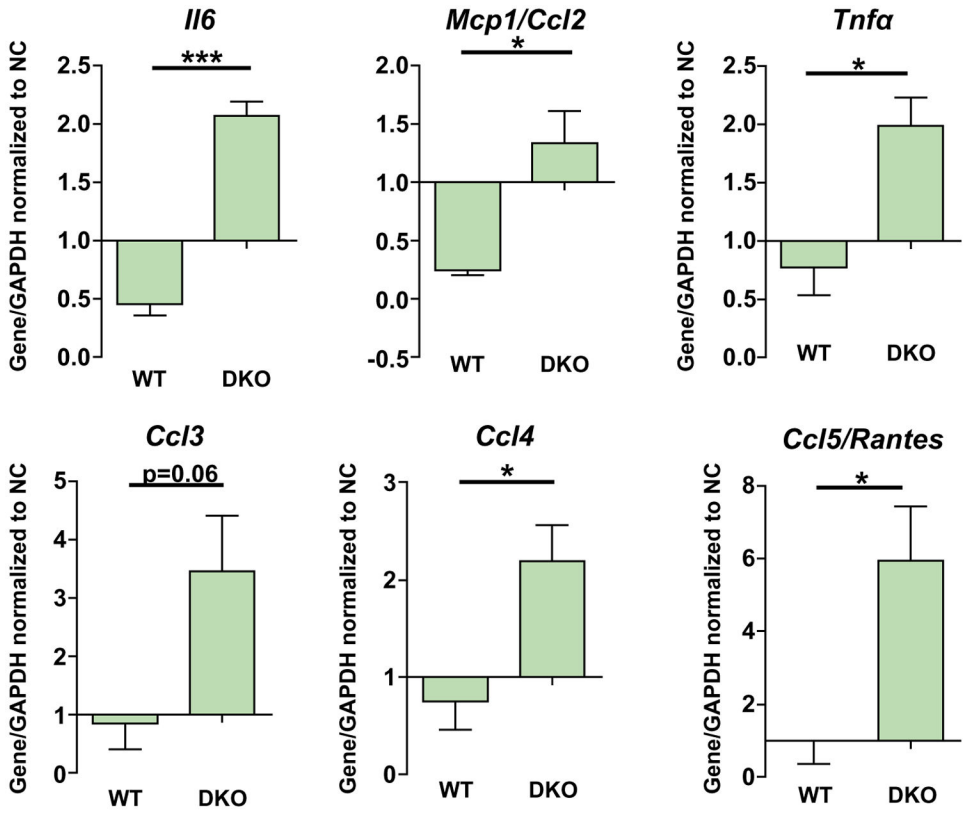

FIG. 8.

DKO ERCs induce BMDM to express proinflammatory genes. BMDM from WT mice were cocultured with WT or DKO ERCs or with ERC culture medium (negative control) for 12 hours. Expression of proinflammatory cytokines in BMDM was measured by quantitative real-time PCR. Bars represent the average fold change over the housekeeping gene (GAPDH) normalized to negative control (n = 3-4). Data are expressed as mean ± SEM. *$P < 0.05$, ***$P < 0.005$. Abbreviations: GAPDH, glyceraldehyde 3-phosphate dehydrogenase; Mcp1, monocyte chemoattractant protein 1; NC, negative control.